nature publishing group
Open

Melanocortin Receptor 4 Deficiency Affects Body Weight Regulation, Grooming Behavior, and Substrate Preference in the Rat

Joram D. Mul[1,4], Ruben van Boxtel[1,4], Dylan J.M. Bergen[1], Maike A.D. Brans[2], Jan H. Brakkee[2], Pim W. Toonen[1], Keith M. Garner[2], Roger A.H. Adan[2] and Edwin Cuppen[1,3]

Obesity is caused by an imbalance between energy intake and expenditure and has become a major health-care problem in western society. The central melanocortin system plays a crucial role in the regulation of feeding and energy expenditure, and functional loss of melanocortin receptor 4 (MC4R) is the most common genetic cause of human obesity. In this study, we present the first functional *Mc4r* knockout model in the rat, resulting from an *N*-ethyl-*N*-nitrosourea mutagenesis–induced point mutation. *In vitro* observations revealed impaired membrane-binding and subsequent nonfunctionality of the receptor, whereas *in vivo* observations showed that functional loss of MC4R increased body weight, food intake, white adipose mass, and changed substrate preference. In addition, intracerebroventricular (ICV) administration of Agouti-Related Protein$_{79–129}$ (AgRP$_{79–129}$), an MC4R inverse agonist, or Melanotan-II (MTII), an MC4R agonist, did affect feeding behavior in wild-type rats but not in homozygous mutant rats, confirming complete loss of MC4R function *in vivo*. Finally, ICV administration of MTII induced excessive grooming behavior in wild-type rats, whereas this effect was absent in homozygous mutant rats, indicating that MTII-induced grooming behavior is exclusively regulated *via* MC4R pathways. Taken together, we expect that the MC4R rat model described here will be a valuable tool for studying monogenic obesity in humans. More specifically, the relative big size and increased cognitive capacity of rats as compared to mice will facilitate complex behavioral studies and detailed mechanistic studies regarding central function of MC4R, both of which ultimately may help to further understand the specific mechanisms that induce obesity during loss of MC4R function.

Obesity (2012) **20,** 612–621. doi:10.1038/oby.2011.81

INTRODUCTION

Melanocortin receptor 4 (MC4R) is a key element in hypothalamic control of short- and long-term energy homeostasis by integrating signals provided by α-melanocyte-stimulating hormone (α-MSH), an MC4R agonist, and Agouti-Related Peptide (AgRP), an MC4R inverse agonist (1–4). The central melanocortin system contains several neuronal circuits including leptin-sensitive neurons expressing proopiomelanocortin (*Pomc*) or *Agrp* in the arcuate nucleus, brainstem neurons expressing *Pomc*, and downstream targets of these neurons expressing melanocortin receptor 3 (*Mc3r*) and *Mc4r* (5). In short, a positive energy state activates anorexigenic α-MSH signaling and represses expression of orexigenic *Agrp*, thus increasing energy expenditure and lowering caloric intake through increased downstream MC3R and MC4R signaling, whereas a negative energy state triggers opposite events.

In humans, haploinsufficiency of *Mc4r* is the most common monogenic cause of severe obesity, accounting up to ~3% of all cases (6–9). Human genome-wide association studies have demonstrated that single-nucleotide polymorphisms in *MC4R* or genetic variances near *MC4R* are highly associated with increased BMI, adipose mass, early-onset obesity, and risk to develop obesity (10–13). Moreover, about 150 *MC4R* mutations, predominantly with a negative effect on MC4R function, have been reported to date in humans (reviewed in ref. 5). In addition, targeted disruption of *Mc4r* in mice resulted in increased food intake, body weight, body length, serum hormone levels, lean mass, and white adipose tissue (WAT) levels (14). Finally,

The first two authors contributed equally to this work.
[1]Hubrecht Institute-KNAW & University Medical Center Utrecht, Utrecht, The Netherlands; [2]Rudolf Magnus Institute of Neuroscience, Department of Neuroscience and Pharmacology, University Medical Center Utrecht, Utrecht, The Netherlands; [3]University Medical Center Utrecht, Department of Medical Genetics, Utrecht, The Netherlands; [4]Present address: Metabolic Diseases Institute, Department of Medicine, University of Cincinnati, Cincinnati, Ohio, USA (J.D.M.); Molecular Immunology Laboratory, Department of Immunology, University Medical Center Utrecht, Utrecht, The Netherlands (R.v.B.). Correspondence: Edwin Cuppen (e.cuppen@hubrecht.eu)

Received 21 December 2010; accepted 4 March 2011; published online 28 April 2011. doi:10.1038/oby.2011.81

these *Mc4r*$^{-/-}$ mice show an identical clinical syndromal picture as compared to human patients with *mc4r* haploinsufficiency (14–16).

In this study, we present the first functional knockout rat model for *Mc4r*, which was identified in a recent *N*-ethyl-*N*-nitrosourea (ENU)-mutagenesis screen in our lab (17). We observed an ENU-induced premature stop codon in helix 8 of the G-protein-coupled receptor (*Mc4r*^{K314X}), and we hypothesized that this mutation would result in loss of function as the mutated MC4R^{K314X} misses, amongst other important amino acids, two C-terminal isoleucines that are essential for correct receptor function (18). Therefore, we tested the functionality of the mutated receptor *in vitro*, and performed a basic characterization of rats heterozygous (*Mc4r*$^{+/K314X}$) and homozygous (*Mc4r*$^{K314X/K314X}$) for the mutation. Furthermore, we tested the effect of Agouti-Related Protein$_{79–129}$ (AgRP$_{79–129}$), an MC4R inverse agonist, on feeding behavior and the effect of Melanotan-II (MTII; ref. 19), an MC4R agonist, on feeding behavior and grooming behavior in *Mc4r*$^{K314X/K314X}$ rats. Finally, we investigated whether *Mc4r*$^{K314X/K314X}$ rats demonstrated a changed substrate preference when offered a high-fat/high-sucrose (HFHS) choice diet.

METHODS AND PROCEDURES

Animals

The Animal Care Committee of the Royal Dutch Academy of Science approved all experiments according to the Dutch legal ethical guidelines. The *Mc4r* mutant rat line (*Mc4r*^{1Hubr}) was generated by target-selected ENU-driven mutagenesis (see ref. 17), and high-throughput resequencing of genomic target sequences in progeny from mutagenized rats (Wistar/Crl background) revealed an ENU-induced premature stop codon in helix 8 (K314X) of *Mc4r*. The heterozygous mutant rat was backcrossed to wild-type Wistar background for six generations to eliminate confounding effects from background mutations induced by ENU as described before (20). To further control for possible contributions of confounding mutations, we repeated several measurements in different outcross generations and could replicate previous findings in each generation. Additionally, we always compared littermates that were generated by crossing *Mc4r*$^{+/K314X}$ rats. Experimental rats were obtained at the expected Mendelian frequency. *Mc4r*$^{K314X/K314X}$ rats were viable into adulthood and appeared phenotypically normal despite their increased body weight. Two rats were housed together, unless noted otherwise, under controlled experimental conditions (12-h light/dark cycle, light period 0600–1800 hours, 21 ± 1 °C, ~60% relative humidity). Standard fed chow diet (semi high-protein chow: RM3, 27% crude protein, and 12% fat, 3.33 kcal/g AFE; SDS, Witham, UK) and water was provided *ad libitum* unless noted otherwise. All rats had access to home-cage enrichment (red rat retreat; Plexx, Elst, the Netherlands and aspen gnaw brick; Technilab-BMI, Someren, the Netherlands), unless noted otherwise. Only male rats were used in this study.

Rat genotyping

DNA isolation and genotyping were performed as described previously (21). In brief, a fragment of *Mc4r*, containing the ENU-induced mutation was amplified using gene-specific primers (forward (F):CCCAA CTTCT ACAGG CAGAC; reverse (R): TGGTA ATGAG GCAGA TGATG) and a touchdown PCR cycling program (92 °C for 60 s; 12 cycles of 92 °C for 20 s, 65 °C for 20 s with a decrement of 0.6 °C per cycle, 72 °C for 30 s, followed by 20 cycles of 92 °C for 20 s, 58 °C for 20 s, and 72 °C for 30 s; 72 °C for 180 s; GeneAmp9700; Applied Biosystems, Foster City, CA). The PCR reactions were diluted with 25 µl water, and 1 µl was used as template for the dideoxy sequencing reactions, which were preformed according to the manufacturer instructions (Applied Biosystems). Sequencing products were purified using Sephadex G50 (superfine, coarse; Sigma, Zwijndrecht, the Netherlands) mini-columns and analyzed on a 96-capillary 3730XL DNA analyzer (Applied Biosystems). Sequences were analyzed for polymorphisms using polyphred (22) and manual inspection of the mutated position. All pups were genotyped around postnatal day (PND) 21. Genotypes were confirmed when experimental procedures were completed.

In vitro membrane expression and cAMP response

N-terminally hemagglutinin (HA)-tagged MC4R^{WT} and MC4R^{K314X} constructs were cloned into the pcDNA3.1 expression vector (Invitrogen, Carlsbad, CA) and membrane expression of the HA-tagged receptors was tested in HeLa cells as described before (17). *In vitro* membrane expression data shown are general representation of observed results. MC4R^{K314X} functionality was tested using a *LacZ* reporter-gene assay as previously described (23). Briefly, HEK293 cells co-transfected with either *Cre::LacZ* and pcDNA3.1-HA-Mc4r^{WT} or with *Cre::LacZ* and pcDNA3.1-HA-Mc4r^{K314X} were allowed to grow in a 96-well plate for 48 h. Subsequently, cells were incubated with the appropriate concentration α-MSH or forskolin (intrinsic activation of cyclic AMP (cAMP), used as positive control) in serum free Dulbecco's modified Eagle's medium. Dulbecco's modified Eagle's medium was discarded after 5 h of incubation, lysis buffer was added, and plates were stored directly at −20 °C. After defrosting the suspension, the substrate mix was added (1.6 g/liter *o*-nitrophenyl β-D-galactopyranoside with β-mercaptoethanol (67.5 mmol/l), and $MgCl_2$ (1.5 mmol/l) in phosphate-buffered saline). Light absorbance was measured at 405 nm. The experiment was done in *triplo* per genotype and data is shown as average.

A receptor-binding competition assay using ^{125}I-NDP-α-MSH

In vitro MC4R binding was measured by co-transfecting HEK293 cells with 7 µg of pcDNA-HA-MC4R^{WT} or pcDNA-HA-MC4R^{K314X} in combination with 400 ng TK-Renilla luciferase DNA. After 24 h of incubation, cells were split in two aliquots and one aliquot was treated with the indicated concentration of competing cold [Nle^4, D-Phe^7]-α-MSH (NDP-α-MSH) in combination with a stable concentration of the radio ligand ^{125}I-NDP-α-MSH (7,000 counts per minute per well; both peptides diluted in Ham's F10 medium (Gibco) with 2.5 mmol/l $CaCl_2$, 0.25% bovine serum albumin, and 200 KIU/ml aprotinin supplement) supplemented with Tris-buffered saline containing 2.5 mmol/l $CaCl_2$ for 30 min at room temperature. The second aliquot was used to measure Renilla activity for transfection efficiency calculation and raw data corrections. The data are expressed in counts per minutes (cpm) and was measured in a lysed (using 1 M sodium hydroxide) cell suspension using a γ-counter. The experiment was done *in triplo* per genotype and data are shown as average.

Body composition

Starting at PND 33, rat body weight was measured weekly. For relative body weight, average body weight of wild-type rats was set at 100% and average body weight of *Mc4r*$^{K314X/K314X}$ rats was expressed as a percentage of average wild-type body weight. At PND 96, left and right subcutaneous and perirenal WAT fat pads were isolated and weighted. Subsequently, perirenal WAT pads were fixed in 4% formaldehyde, rotated overnight at room temperature, washed with phosphate-buffered saline, and rinsed in 70% ethanol for at least 1 h. WAT pads were processed to paraffin (96% ethanol for 2 h, 2× 100% ethanol for 1.5 h, xylene for 2 h and embedded in paraffin overnight), cut to 14 µm sections, and stained with eosin. Adipocyte size of the perirenal WAT was calculated using NIH Image J software (Bethesda, MD). Per genotype, three rats were analyzed (10 pictures per rat, each picture taken at a different morphological site).

Plasma hormone levels

At PND 96, blood samples were collected after decapitation. Plasma insulin and leptin levels were measured as described before (20).

Basal food intake measurements
Starting at postnatal day (PND) 49, rats were housed individually and food intake, water intake, and body weight were measured during PND 56–63.

Bomb calorimetry
During basal food intake measurements, fecal samples were collected between PND 59 and 63, freeze-dried, and analyzed for gross energy content using adiabatic bomb calorimetry (IKA Calorimeter System C4000; IKA, Heitersheim, Germany). The feed conversion efficiency was calculated as the body weight gain (g) divided by the effective energy intake (kcal; kcal ingested minus kcal lost in feces) per day.

Ambulatory activity
Starting at PND 70, rats were allowed to habituate to the experimental room for 24 h before placement in a Phenotyper home-cage monitoring system (Noldus Information Technology, Wageningen, the Netherlands). After 20 h of acclimatization to the Phenotyper cages, basal ambulatory activity was measured during 24 h. Data were analyzed using Ethovision software (Noldus Information Technology) in combination with in-house developed software.

Hypothalamic mRNA expression
Ad libitum-fed rats were killed at PND 182 during the early afternoon and the hypothalamus was rapidly dissected and snap-frozen in liquid nitrogen. Hypothalamic mRNA expression was measured exactly as described before (20), with the addition that DNA was removed from the RNA samples using DNAse (Promega) as described by the manufacturer (*Mc3r* is a single exon gene). Primers were designed using SciTools PrimerQuest (IDT): *Cyclophilin* (F: ACTT CATG ATCC AGGG TGGA GACT; R: AAGT TCTC ATCT GGGA AGCG CTCA), *Pomc* (F: TCCA TAGA CGTG TGGA GCTG GT; R: TTCA TCTC CGTT GCCT GGAA ACAC), *Cartpt* (F: TGGA CATC TACT CTGC CGTG GAT; R: TTCC TGCA GCGC TTCA ATCT GCAA), *Npy* (F: AGAG GACA TGGC CAGA TACT ACTC; R: AATC AGTG TCTC AGGG CTGG ATC), and *Mc3r* (F: CATG TACT TCTT CCTG TGCA GCCT; R: AAGG TCAG GGAG TCGC TGTT GATA) Average $Mc4r^{K314X/K314X}$ rat gene expression from the two experiments is expressed as a percentage of average wild-type rat gene expression.

ICV cannula implantation
Starting at PND 89, rats were allowed to habituate to the experimental room and housed individually. The next day, rats were anesthetized by subcutaneous injection of Hypnorm (1.0 ml/kg; 10 mg/ml fluanisone, 0.315 mg/ml fentanyl citrate; Janssen Animal Health, Beerse, Belgium) and pain was reduced by Carprofen (Pfizer Animal Health, New York, NY) intramuscularly administered (0.1 ml/100 g body weight). A 16-mm stainless gauge was implanted in the lateral ventricle (stereotaxic coordinates: 1.0 mm posterior and 2.0 mm lateral of the bregma) as described earlier (24). After surgery, rats received two intraperitoneal injections of 3 ml saline to aid recovery. Rats were allowed to recover for 9 days, during which rats were handled frequently.

ICV administration of MTII and $AgRP_{79–129}$
At PND 99, body weight was measured and rats were placed on a caloric restriction for 6 h (12 till 6 PM). Directly after start of the dark phase (6 PM), rats were injected with 3 µl saline. Subsequently, food and water intake was measured for 22 h after which the body weight was measured again at the end of the experiment. This paradigm was repeated with the administration of 1 nmol/l MTII (PND 103; Tocris Bioscience, Bristol, UK) and 1 nmol/l $AgRP_{79–129}$ (PND 106; Phoenix Pharmaceuticals, Burlingame, CA). Experimental peptides were dissolved in 3 µl saline.

Grooming assay
The grooming assay was done as described before (25). Briefly, at PND 109 rats were transported from the in-house animal facility, to an observation room 2 h before start of the behavioral test, during which rats had no cage enrichment, or access to food or water. Grooming was induced by ICV administration of 1 nmol/l MTII (dissolved in 3 µl saline). In our experiments, the observation cage consisted of a Phenotyper home-cage monitoring system (Noldus Information Technology) in which rats were placed immediately after the ICV injection. Observation started 15 min after the injection and continued for 50 min. Grooming was scored every 15 s during 50 min resulting in maximal 200 grooming scores. The grooming elements vibrating, face washing, body and genital grooming, body licking, scratching, and paw licking were scored. The grooming tests were performed during the early afternoon. After experimental handling, the rats were killed and correct implantation of the ICV cannula was checked using a Methylene Blue injection. Only data from rats with a correct cannula were used.

HFHS-choice diet
Rats were individually housed at PND 69 and received *ad libitum* access to standard fed semi high-protein diet and water. Body weight and food intake was monitored every 2 days for 10 days (between PND 69 and 79). At PND 79, rats received access to a food dispenser with standard semi high-protein diet, a food dispenser with HF diet (45%-AFE, 20% crude protein, 45% fat, and 35% carbohydrates; 4.54 kcal/g AFE; SDS), one bottle of water, and one bottle of 30% sugar water (1.2 kcal/g). After 6 days of acclimation to the novel diets, body weight and food intake was monitored every 2 days for 10 days (between PND 85 and 95). Dispensers and bottles were swapped every 2 days to control for side-preference effects.

Data analysis
All data are shown as mean ± SEM. All data were analyzed using a commercially available statistical program (SPSS for Macintosh, version 16.0) and were controlled for normality and homogeneity. **Figures 1d–f, 2a, 4b,** and **8a,b** were analyzed using repeated measures analysis, followed by Bonferroni *post hoc* analyses if significant overall interactions were observed. **Figure 3a–f** was analyzed using one-way ANOVA, followed by Bonferroni *post hoc* analyses if significant overall interactions were observed. **Figure 6a,b** was analyzed using two-way ANOVA, followed by Bonferroni *post hoc* analyses if significant overall interactions were observed. All other data were analyzed using a Student's *t*-test. The null hypothesis was rejected at the 0.05 level.

RESULTS
The $Mc4r^{K314X}$ mutation results in loss of function
We have recently described a mutation in the *Mc4r* gene in the rat ($Mc4r^{K314X}$), which generates a premature stop codon and an 18-amino acid truncation in helix 8 of the receptor, thereby removing the C-terminus, which is essential for receptor cell surface localization (**Figure 1a**; refs. 17,18). Indeed, whereas HA-tagged $MC4R^{WT}$ was clearly detectable at the plasma membrane of HeLa cells, HA-tagged $MC4R^{K314X}$ could not be detected at the plasma membrane (**Figure 1b**), confirming earlier observations (17). Permeabilization of transfected cells reconfirmed the presence of approximately equal expression levels of both wild-type and mutant HA-MC4R fusion proteins (**Figure 1c**), indicating that mutant MC4R is probably synthesized but fails to be transported to the plasma membrane where it normally performs its function.

Using an *in vitro* cAMP assay, we show that HEK293 cells transfected with HA-tagged $Mc4r^{K314X}$ were unable to activate cAMP after addition of α-MSH, whereas cells transfected with HA-tagged $Mc4r^{WT}$ show a dose-dependent response (**Figure 1d**). The statistical analysis for cAMP readout after α-MSH treatment revealed a significant effect of dilution

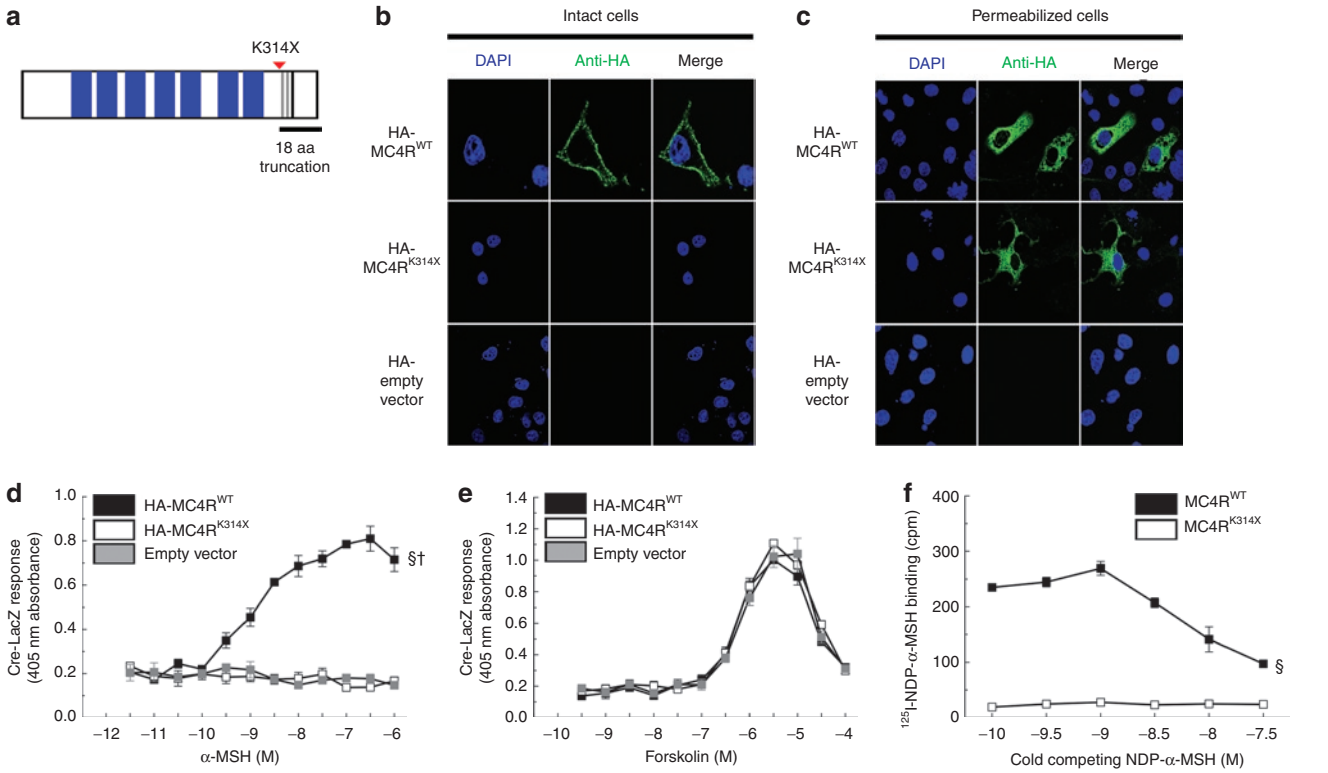

Figure 1 The *MC4R*^{K314X} mutation results in loss of function *in vitro*. (**a**) Schematic overview of MC4R; blue: transmembrane domains; grey: isoleucine residue; black; palmitoylated cysteine residue (for a more detailed schematic overview, see ref. 17). (**b**) *In vitro* protein localization assays in transfected HeLa cells reveal plasma membrane localization for wild-type MC4R, but not for the mutated version of melanocortin 4 (MC4R). Membrane localization was detected using N-terminally hemagglutinin (HA)-tagged fusion constructs and extracellular availability of the HA tag in intact cells. (**c**) Both wild-type and mutant fusion proteins can be detected in fixed and permeabilized HeLa cells, indicating that the mutant fusion protein is expressed, but fails to properly insert into the plasma membrane. (**d**). Dose-response curve of α-melanocyte-stimulating hormone (α-MSH) showing its ability to stimulate HEK293 cells expressing the wild-type MC4R fusion protein and a cyclic AMP (AMP)-sensitive reporter gene. This effect was absent in HEK293 cells expressing the mutant MC4R fusion protein and a cAMP-sensitive reporter gene or in HEK293 cells expressing an empty vector and a cAMP-sensitive reporter gene. (**e**) Dose-response curve of forskolin treatment as a positive control for MC4R construct and *Cre::LacZ* transfection of HEK293 cells. (**f**) Intact HEK293 cells transfected with the mutant receptor (MC4R^{K314X}) were not able to bind its radioactive ligand (^{125}I-NDP-α-MSH), whereas cells transfected with the wild-type receptor (MC4R^{WT}) demonstrated a detectable signal. Increasing concentrations of cold NDP-α-MSH competed with the radioactive agonist and resulted in an expected dropping curve in cells transfected with MC4R^{WT} ($^{§}P < 0.001$, MC4R^{WT} vs. MC4R^{K314X}, $^{†}P < 0.001$, MC4R^{WT} vs. empty vector by Bonferroni *post hoc* analysis). Data are shown as mean ± SEM.

($F_{(11,99)} = 22$; $P < 0.001$), of genotype ($F_{(2,9)} = 418$; $P < 0.001$), and a dilution × genotype interaction ($F_{(22,99)} = 34$; $P < 0.001$; **Figure 1d**). To control whether the HA tag could have an effect on the assay we measured α-MSH response of HEK293 cells transfected with non-HA-tagged Mc4r^{WT}, which showed an equal cAMP readout as compared to HA-tagged Mc4r^{WT} transfected cells when treated with the same dilution series of α-MSH or forskolin (data not shown). This demonstrates that the HA tag did not influence wild-type receptor activity. Furthermore, treatment with forskolin shows the same degree of cAMP activation in all tested conditions, demonstrating that an equal number of cells were transfected with the different expression vectors (**Figure 1e**). The statistical analysis for cAMP readout after forskolin treatment revealed a significant effect of dilution ($F_{(7,63)} = 272$; $P < 0.001$), but no effect of genotype ($F_{(2,9)} = 3$; $P = 0.11$), and no dilution × genotype interaction ($F_{(14,63)} = 1$; $P = 0.44$; **Figure 1e**).

Finally, we demonstrated that HEK293 cells transfected with HA-Mc4r^{K314X} were unable to bind radioactive ^{125}I-NDP-α-MSH during a receptor-binding competition assay whereas a significant signal was detected for cells transfected with HA-Mc4r^{WT} (**Figure 1f**). The statistical analysis for ^{125}I-NDP-α-MSH binding after cold NDP-α-MSH treatment revealed a significant effect of dilution ($F_{(4,17)} = 40$; $P < 0.001$), of genotype ($F_{(1,4)} = 627$; $P < 0.001$), and a dilution × genotype interaction ($F_{(4,17)} = 40$; $P < 0.001$; **Figure 1f**).

The *Mc4r*^{K314X} mutation results in obesity

Body weight analysis of rats during development revealed that *Mc4r*$^{K314X/K314X}$ rats developed early-onset obesity whereas *Mc4r*$^{+/K314X}$ rats developed late-onset obesity as compared to wild-type siblings (**Figure 2a,b**). The statistical analysis for body weight revealed a significant effect of time ($F_{(9,261)} = 2262$; $P < 0.001$), an effect of genotype ($F_{(2,29)} = 20$; $P < 0.001$), and a time × genotype interaction ($F_{(18,261)} = 38$; $P < 0.001$; **Figure 2a**). At PND 96, average body weight of *Mc4r*$^{+/K314X}$ and *Mc4r*$^{K314X/K314X}$ rats was 493 ± 8 g (116 ± 2%) and 602 ± 12 g (141 ± 3%), respectively, as compared to wild-type siblings (426 ± 15 g;

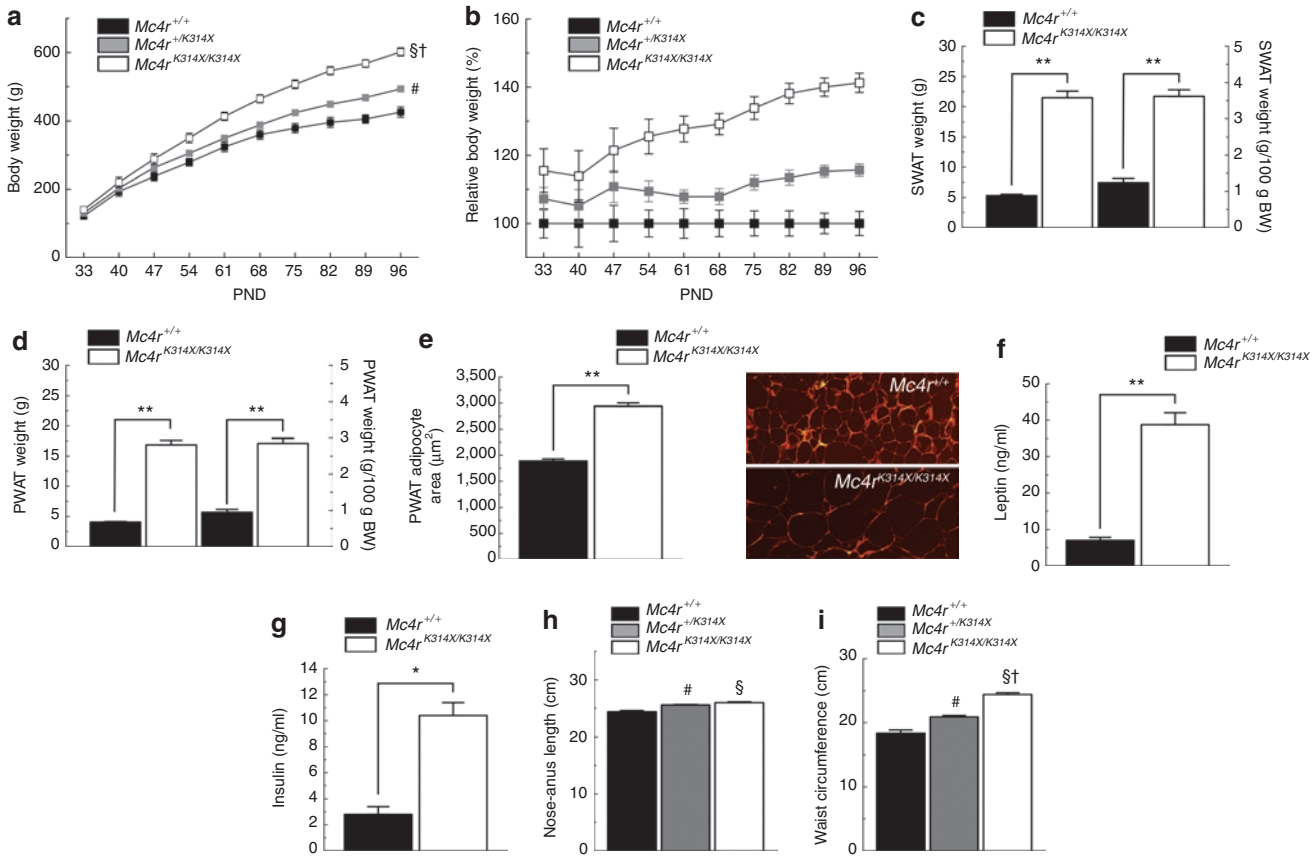

Figure 2 The *Mc4r*^{K314X} mutation induces obesity. (**a**) Body weight and (**b**) relative body weight of *Mc4r*$^{+/+}$ ($n = 6$), *Mc4r*$^{+/K314X}$ ($n = 14$), and *Mc4r*$^{K314X/K314X}$ ($n = 12$) rats during development. (**c**) Absolute SWAT weight (left axis) and normalized for body weight (right axis), and (**d**) absolute PWAT weight (left axis) and normalized for body weight (right axis) of *Mc4r*$^{+/+}$ ($n = 3$) and *Mc4r*$^{K314X/K314X}$ ($n = 8$) rats at PND 96. (**e**) PWAT adipocyte cell area of *Mc4r*$^{+/+}$ and *Mc4r*$^{K314X/K314X}$ rats ($n = 3$ per genotype) at PND 96 (left) and representative cross-sections of perirenal fat pads from *Mc4r*$^{+/+}$ and *Mc4r*$^{K314X/K314X}$ rats at PND 96, respectively (×200 magnification; right). (**f**) Leptin and (**g**) insulin plasma levels of nonstarved *Mc4r*$^{+/+}$ ($n = 3$) and *Mc4r*$^{K314X/K314X}$ ($n = 8$) rats at PND 96. (**h**) Nose–anus length and (**i**) waist circumference of *Mc4r*$^{+/+}$ ($n = 6$), *Mc4r*$^{+/K314X}$ ($n = 8$), and *Mc4r*$^{K314X/K314X}$ ($n = 12$) rats at PND 96 ($^{\S}P < 0.001$, *Mc4r*$^{K314X/K314X}$ vs. *Mc4r*$^{+/+}$, $^{\dagger}P < 0.001$, *Mc4r*$^{K314X/K314X}$ vs. *Mc4r*$^{+/K314X}$, $^{\#}P < 0.001$, *Mc4r*$^{+/K314X}$ vs. *Mc4r*$^{+/+}$ by Bonferroni *post hoc* analysis; $^{*}P < 0.005$, $^{**}P < 0.001$ by Student's *t*-test). Data are shown as mean ± SEM.

Figure 2a,b). *Mc4r*$^{K314X/K314X}$ rats displayed increased subcutaneous and perirenal WAT mass as compared to wild-type siblings (405 ± 21% and 415 ± 18%, respectively; Figure 2c,d), both of which remained increased when normalized for body weight (291 ± 15% and 299 ± 15%, respectively; Figure 2c,d). Moreover, *Mc4r*$^{K314X/K314X}$ rats demonstrated increased perirenal adipocyte cell size (Figure 2e), increased plasma leptin levels (553 ± 47%; Figure 2f), and increased plasma insulin levels (372 ± 36%; Figure 2g) as compared to wild-type siblings. Finally, an increase in body weight in *Mc4r*$^{+/K314X}$ and *Mc4r*$^{K314X/K314X}$ rats at PND 96 was accompanied by an increase in body length and waist circumference (Figure 2h,i).

The *Mc4r*^{K314X} mutation results in hyperphagia

During postnatal week 9 (PND 56–63), the average body weight of *Mc4r*$^{K314X/K314X}$ rats was increased as compared to wild-type siblings (125 ± 3% as compared to wild-type rats), whereas body weights did not differ significantly between *Mc4r*$^{+/K314X}$ and wild-type rats (98 ± 1% as compared to wild-type rats; Figure 3a). Both *Mc4r*$^{+/K314X}$ and *Mc4r*$^{K314X/K314X}$ rats demonstrated increased food intake as compared to wild-type siblings, although the difference between *Mc4r*$^{+/K314X}$ and wild-type rats was not significant (Figure 3b). Moreover, when food intake was normalized for body weight, both *Mc4r*$^{+/K314X}$ and *Mc4r*$^{K314X/K314X}$ rats were hyperphagic as compared to wild-type siblings (Figure 3c). *Mc4r*$^{K314X/K314X}$ rats also consumed more water as compared to wild-type siblings (see **Supplementary Figure S1** online).

During PND 56–59, fecal output and fecal energy loss of *Mc4r*$^{K314X/K314X}$ rats were increased as compared to *Mc4r*$^{+/K314X}$ and wild-type siblings, whereas fecal output did not differ significantly between *Mc4r*$^{+/K314X}$ and wild-type rats (Figure 3d,e). During these 3 days, the feed conversion efficiency did not differ significantly between wild-type, *Mc4r*$^{+/K314X}$, and *Mc4r*$^{K314X/K314X}$ rats (Figure 3f).

The *Mc4r*^{K314X} mutation decreases ambulatory activity

During postnatal week 10, total ambulatory activity of *Mc4r*$^{K314X/K314X}$ rats was decreased during the light phase, the dark phase, and during 24 h as compared to wild-type siblings

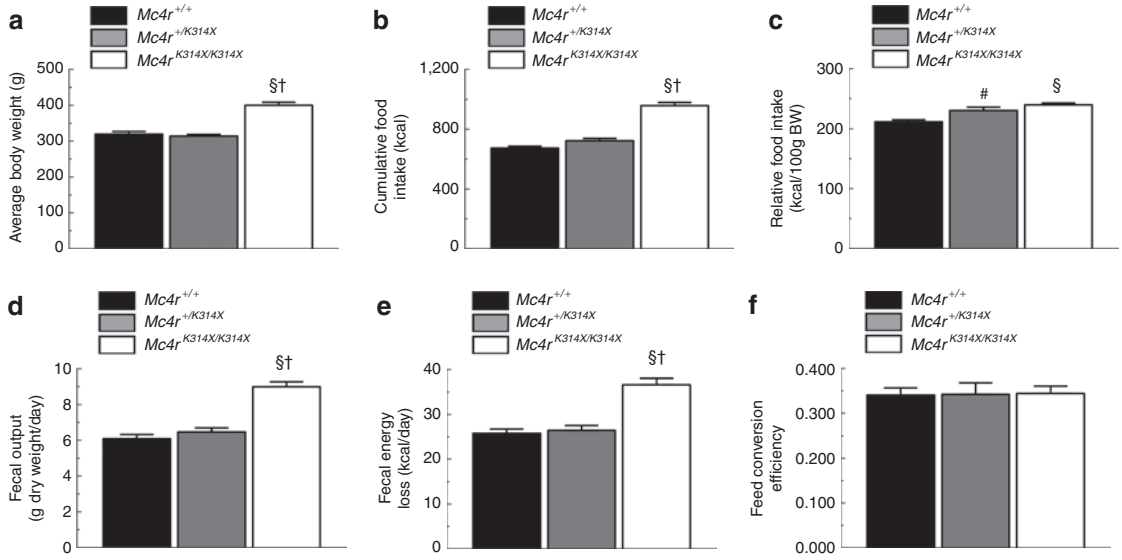

Figure 3 The *Mc4r*^{K314X} mutation induces hyperphagia. (**a**) Average body weight, (**b**) cumulative food intake, and (**c**) cumulative food intake normalized for average body weight of *Mc4r*$^{+/+}$ ($n = 9$), *Mc4r*$^{+/K314X}$ ($n = 6$), and *Mc4r*$^{K314X/K314X}$ ($n = 9$) rats during postnatal week 9 (PND 56–63). (**d**) Fecal output (g dry weight per day), (**f**) energy loss through feces (kcal per day), and (**e**) feed conversion efficiency (g weight gain divided by effective caloric intake) of *Mc4r*$^{+/+}$ ($n = 9$), *Mc4r*$^{+/K314X}$ ($n = 6$), and *Mc4r*$^{K314X/K314X}$ ($n = 9$) rats during PND 59–63 ($^{§}P < 0.001$, *Mc4r*$^{K314X/K314X}$ vs. *Mc4r*$^{+/+}$, $^{†}P < 0.001$, *Mc4r*$^{K314X/K314X}$ vs. *Mc4r*$^{+/K314X}$, $^{\#}P < 0.01$, *Mc4r*$^{+/K314X}$ vs. *Mc4r*$^{+/+}$ by Bonferroni *post hoc* analysis). Data are shown as mean ± SEM.

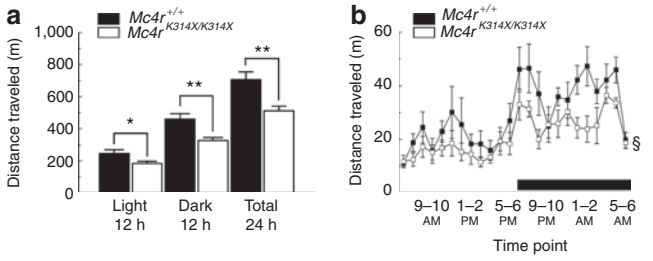

Figure 4 The *Mc4r*^{K314X} mutation decreases ambulatory activity. (**a**) Cumulative ambulatory activity during light phase (12 h), dark phase (12 h), and per whole day (24 h) and (**b**) ambulatory activity represented per hour of 10-week-old *Mc4r*$^{+/+}$ and *Mc4r*$^{K314X/K314X}$ rats ($n = 8$ per genotype; $^{*}P < 0.05$, $^{**}P < 0.005$ by Student's *t*-test; $^{§}P < 0.05$, *Mc4r*$^{K314X/K314X}$ vs. *Mc4r*$^{+/+}$ by Bonferroni *post hoc* analysis). Data are shown as mean ± SEM.

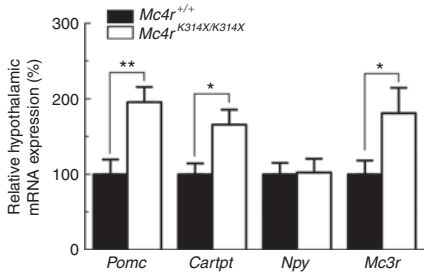

Figure 5 The *Mc4r*^{K314X} mutation affects hypothalamic gene expression. Relative hypothalamic expression of *Npy* is unchanged, whereas expression of *Pomc*, *Cartpt*, and *Mc3r* is increased in adult *ad libitum*-fed *Mc4r*$^{K314X/K314X}$ rats as compared to *Mc4r*$^{+/+}$ rats ($n = 5$ per genotype; $^{*}P < 0.05$, $^{**}P < 0.005$ by Student's *t*-test). Data are shown as mean ± SEM.

(Figure 4a,b). The statistical analysis for 24 h ambulatory activity revealed a significant effect of time ($F_{(16,217)} = 7$; $P < 0.001$), of genotype ($F_{(1,14)} = 13$; $P < 0.005$), but no time × genotype interaction ($F_{(16,217)} = 1$; $P = 0.61$; Figure 4b).

The *Mc4r*^{K314X} mutation affects hypothalamic gene expression

Because the hypothalamus is an important brain region regulating energy balance, gene expression of *Pomc*, cocaine-, and amphetamine-regulated transcript (*Cartpt*), neuropeptide-Y (*Npy*), and *Mc3r* was investigated in hypothalamus samples of *ad libitum*-fed adult rats. At PND 182, relative hypothalamic gene expression of *Pomc* and *Cartpt*, both food intake-suppressing genes, was upregulated, whereas relative expression of *Npy*, a food intake-stimulating gene, was unchanged in *Mc4r*$^{K314X/K314X}$ rats as compared to wild-type rats (Figure 5). In addition, relative hypothalamic gene expression of *Mc3r* was increased in *Mc4r*$^{K314X/K314X}$ rats as compared to wild-type rats (Figure 5).

Pharmacological manipulation of the melanocortin system *in vivo*

Activation of MC4R decreases feeding, whereas blockade of MC4R increases feeding (26–28). Therefore, we tested whether *Mc4r*$^{K314X/K314X}$ rats change their feeding behavior in response to ICV administration of $AgRP_{79–129}$, a nonselective MC3R and MC4R inverse agonist, or MTII, a nonselective MC3R and MC4R agonist (19). ICV administration of 1 nmol/l $AgRP_{79–129}$ increased the 22-h cumulative caloric intake in *Mc4r*$^{+/+}$ rats as compared to saline-treated *Mc4r*$^{+/+}$ rats, but had no effect on feeding in *Mc4r*$^{K314X/K314X}$ rats (Figure 6a). Furthermore, ICV administration of 1 nmol/l MTII lowered caloric intake in *Mc4r*$^{+/+}$ rats as compared to saline-treated *Mc4r*$^{+/+}$ rats, but

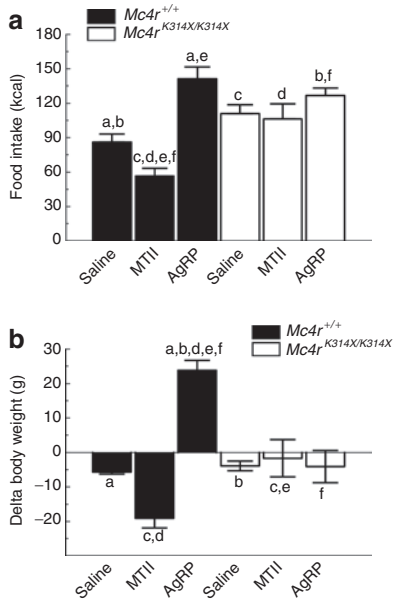

Figure 6 Pharmacological manipulation of the melanocortin system. (**a**) 22-h cumulative caloric intake and (**b**) body weight changes 22 h after intracerebroventricular (ICV) injection of either saline (PND 99), 1 nmol/l MTII (PND 103), or 1 nmol/l $AgRP_{79–129}$ (PND 106) in *Mc4r*$^{+/+}$ ($n = 7$) and *Mc4r*$^{K314X/K314X}$ rats ($n = 8$; bars with the same letter are significantly different, $^{a,c}P < 0.005$, $^{b}P < 0.05$, $^{d}P < 0.01$, $^{e,f}P < 0.001$ (graph a); $^{a,b,d,f}P < 0.001$, $^{c}P < 0.05$, $^{e}P < 0.005$ (graph b) by Bonferroni *post hoc* analysis). Data are shown as mean ± SEM.

again had no effect on feeding in *Mc4r*$^{K314X/K314X}$ rats (Figure 6a). Finally, body weight growth of *Mc4r*$^{+/+}$ rats was positive after $AgRP_{79–129}$ administration and negative after MTII administration, whereas no robust effects were observed in *Mc4r*$^{K314X/K314X}$ rats (Figure 6b).

The *MC4R*^{K314X} mutation abolishes MTII-induced grooming behavior

ICV administration of MTII induces grooming behavior in rats (29). Therefore, we tested whether *Mc4r*$^{K314X/K314X}$ rats increased their grooming behavior in response to ICV MTII administration. ICV administration of 1 nmol/l MTII resulted in excessive grooming behavior during a rat-grooming assay (87 ± 2% of experimental time spent on grooming behavior) in *Mc4r*$^{+/+}$ rats, whereas this excessive behavior was absent in *Mc4r*$^{K314X/K314X}$ rats (8 ± 3% of experimental time spent on grooming behavior; Figure 7). This demonstrates that melanocortin-induced grooming is exclusively mediated by MC4R.

The *MC4R*^{K314X} mutation increases preference for HF substrate

Loss or blockade of MC4R signaling increases HF substrate consumption, changes preference towards an HF diet, and increases appetitive responding for a fat, but not a carbohydrate, reinforcer (30–32). Moreover, *Mc4r*$^{-/-}$ mice increase their body weight markedly as compared to wild-type siblings when fed a moderate-fat diet (33). Here, we gave *Mc4r*$^{+/+}$ and *Mc4r*$^{K314X/K314X}$ rats, raised on a standard chow diet, access to a

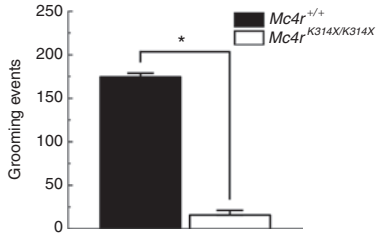

Figure 7 The *Mc4r*^{K314X} mutation abolishes MTII-induced grooming behavior. Number of grooming events measured between 15 and 65 min after intracerebroventricular (ICV) injection of 1 nmol/l MTII in *Mc4r*$^{+/+}$ ($n = 7$) and *Mc4r*$^{K314X/K314X}$ rats at PND 109 ($n = 8$; $^{*}P < 0.001$ by Student's *t*-test). Data are shown as mean ± SEM.

HFHS-choice diet and measured caloric intake and changes in body weight on both diets. *Mc4r*$^{K314X/K314X}$ rats increased their body weight slightly faster, albeit not significantly, during 10 days on a chow diet as compared to wild-type rats. The statistical analysis for body weight growth on a chow diet revealed a significant effect of time ($F_{(4,28)} = 111$; $P < 0.001$), but not of genotype ($F_{(1,7)} = 1$; $P = 0.42$) and no time × genotype interaction ($F_{(4,28)} = 2$; $P = 0.14$; Figure 8a). However, on an HFHS-choice diet, *Mc4r*$^{K314X/K314X}$ rats increased their body weight faster as compared to wild-type rats. The statistical analysis for body weight growth on an HFHS-choice diet revealed a significant effect of time ($F_{(2,12)} = 386$; $P < 0.001$) but not of genotype ($F_{(1,7)} = 1$; $P = 0.39$), and revealed a time × genotype interaction ($F_{(2,12)} = 6$; $P < 0.05$; Figure 8b). *Mc4r*$^{K314X/K314X}$ rats ingested more calories on a standard chow diet as well as on an HFHS-choice diet as compared to wild-type siblings, although this difference was not significant when fed an HFHS-choice diet (Figure 8c). Both genotypes increased their total caloric intake, albeit not significantly, on an HFHS-choice diet as compared to a standard chow diet (*Mc4r*$^{+/+}$: 120.4 ± 3.9%, *Mc4r*$^{K314X/K314X}$: 114.4 ± 4.9%; Figure 8c). Finally, when fed an HFHS-choice diet, *Mc4r*$^{K314X/K314X}$ rats ingested equal calories from the standard chow substrate (*Mc4r*$^{+/+}$: 35.5 ± 1.0%, *Mc4r*$^{K314X/K314X}$: 38.6 ± 6.2%), significantly more calories from the HF substrate (*Mc4r*$^{+/+}$: 42.8 ± 1.6%, *Mc4r*$^{K314X/K314X}$: 53.7 ± 4.3%), and significantly fewer calories from the HS substrate as compared to wild-type rats (*Mc4r*$^{+/+}$: 21.7 ± 1.8%, *Mc4r*$^{K314X/K314X}$: 7.7 ± 2.1%; Figure 8d). This demonstrates that loss of MC4R function changes substrate preference toward HF energy-rich substrates.

DISCUSSION

Taken together, our *in vitro* and *in vivo* data show that the *Mc4r*^{K314X} mutation results in loss of function. We observed that the *Mc4r*^{K314X} mutation abolishes correct membrane localization *in vitro*, and that *Mc4r*$^{K314X/K314X}$ rats demonstrated increased body weight, adipose mass, plasma hormone levels, body length, and basal food intake in combination with decreased ambulatory activity. ICV administration of $AgRP_{79–129}$ or MTII had no robust effect on feeding behavior in *Mc4r*$^{K314X/K314X}$ rats. Furthermore, ICV MTII administration induced excessive grooming behavior in wild-type rats, whereas it had no robust effect on grooming

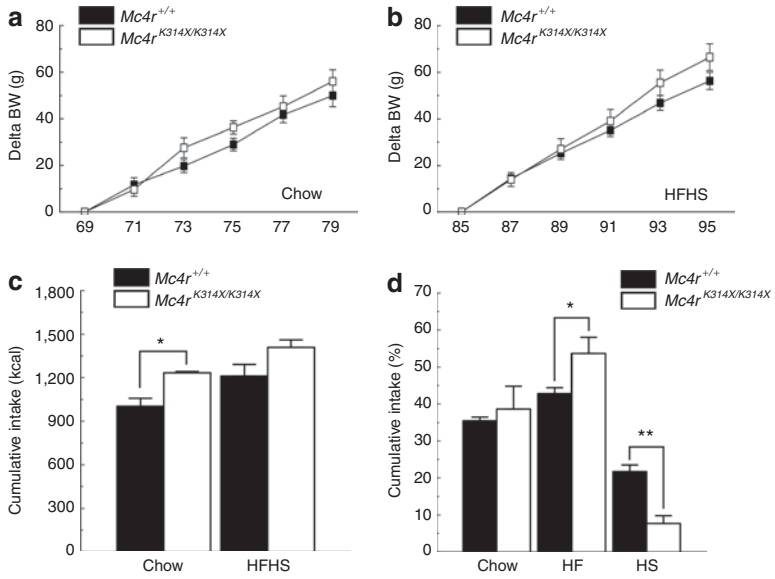

Figure 8 The *Mc4r*^{K314X} mutation changes substrate preference on a high-fat/high-sucrose (HFHS)-choice diet. Increase in body weight of *Mc4r*$^{+/+}$ ($n = 5$) and *Mc4r*$^{K314X/K314X}$ rats ($n = 4$) when fed a (**a**) standard chow diet for 10 days (PND 69–79) or (**b**) an HFHS-choice diet for 10 days (PND 85–95). (**c**) Cumulative caloric intake during 10 days of chow diet or 10 days of an HFHS-choice diet. (**d**) Percentage of total cumulative intake of chow, HF, and HS substrates during access to an HFHS-choice diet (*$P < 0.05$, **$P < 0.005$ by Student's *t*-test). Data are shown as mean ± SEM.

behavior in *Mc4r*$^{K314X/K314X}$ rats. Finally, when offered an HFHS-choice diet, *Mc4r*$^{K314X/K314X}$ rats demonstrated increased preference for an HF substrate in combination with decreased preference for an HS substrate as compared to wild-type rats.

The *in vitro* data obtained with our rat model confirms earlier observations that the C-terminus is essential for correct MC4R cell surface localization, and that subsequent loss of cell surface localization abolishes correct MC4R signaling (18). Moreover, mutation of one of the two C-terminal isoleucines (Ile-317-Thr) in a human proband results in severe overweight (34), indicating that our rat model is a bonafide animal model resembling loss of MC4R function in humans.

Functional loss of MC4R in the rat results in a gene dosage effect on body weight that showed strong overlap with data observed after *Mc4r* disruption in mice (14). Moreover, *Mc4r*$^{K314X/K314X}$ rats demonstrated increased body length, increased food intake, increased plasma insulin and leptin levels, and decreased 24 h ambulatory activity that are also in line with earlier observations in *Mc4r*-null mice (14,35). Finally, ICV administration of $AgRP_{79–129}$ affected feeding behavior and ICV administration of MTII affected feeding and grooming behavior in wild-type rats, both as expected (26,28,29,36), but these effects were absent in *Mc4r*$^{K314X/K314X}$ rats. In sum, our *in vivo* data confirm earlier observations in other rodent models and indicate that the *Mc4r*^{K314X} mutation results in functional loss of MC4R.

Hypothalamic gene expression analysis revealed no significant changes in *Npy* expression, but an increased expression of *Pomc*, *Cartpt*, and *Mc3r* in adult *Mc4r*$^{K314X/K314X}$ rats as compared to wild-type siblings. Increased expression of *Pomc* was not observed in any hypothalamic brain region of *Mc4r*-null mice, whereas increased expression of *Npy* was observed in the dorsal medial hypothalamic nucleus of *Mc4r*-null mice (14). Thus, more specific analysis of gene expression in individual brain regions involved in the regulation of body weight might provide important information on differences between murine and rat models, and the processes underlying MC4R-deficiency-induced obesity.

Mc3r$^{-/-}$ mice on a standard chow diet demonstrate normal body weights, albeit adiposity levels were increased in combination with a lower lean mass as well as a decreased food intake (37). Furthermore, *Mc3r* and *Mc4r* double knockout mice demonstrated heavier body weights than single gene knockouts (37,38). Finally, recently it was shown that MC3R function has an effect, although subtle, on food intake (39). In sum, MC3R, which is generally considered an autoreceptor (40), affects energy homeostasis. Thus, the relative hypothalamic upregulation of *Mc3r* observed in *Mc4r*$^{K314X/K314X}$ rats might result in compensatory effects.

Administration of MTII induces excessive grooming behavior in wild-type rats (29), whereas *Mc4r*$^{K314X/K314X}$ rats do not display excessive MTII-induced grooming behavior. Moreover, the time spent grooming by MTII-injected *Mc4r*$^{K314X/K314X}$ rats did not significantly differ from time spent grooming by saline-injected wild-type rats during a comparable assay (data not shown; ref. 29). This indicates that MTII-induced grooming behavior is activated exclusively through MC4R-specific pathways, and not *via* MC3R-specific pathways.

Loss or blockade of MC4R signaling increases HF substrate consumption, changes preference towards an HF diet, and increases appetitive responding for a fat, but not a carbohydrate, reinforcer in rodents (30–32). Here, we show that functional loss of MC4R in the rat increases preference toward an HF substrate and away from an HS substrate, when offered an HFHS-choice diet. As the mechanism of these motivational changes is not yet fully understood, additional behavioral and molecular

experiments with *Mc4r*$^{K314X/K314X}$ rats on HF diets or on HFHS-choice diets will be of interest. Finally, *Mc4r*$^{-/-}$ mice increased their body weight markedly as compared to wild-type mice when fed a moderate HF diet for 7 days, whereas body weight growth of *Mc4r*$^{K314X/K314X}$ rats on an HFHS-choice diet for 10 days did not differ markedly from wild-type rats. An explanation for this observation might lie in species-specific differences, or in the fact that *Mc4r*$^{K314X/K314X}$ rats had a substrate choice whereas *Mc4r*$^{-/-}$ mice had not. Therefore, a detailed analysis of the homeostatic response of *Mc4r*$^{K314X/K314X}$ rats to a (moderate) HF diet, without access to other substrates, will provide valuable information.

Given the amount of outcrossing to a wild-type background in our experimental *Mc4r*$^{K314X/K314X}$ rats and the strong phenotypic overlap between *Mc4r*$^{K314X/K314X}$ rats and *Mc4r*-null mice, we are confident that the observed phenotypes in *Mc4r*$^{K314X/K314X}$ rats solely result from functional loss of MC4R. Also, an alternative to the conclusion that functional loss of *Mc4r* directly influences energy metabolism is that loss of *Mc4r* could result in a defect in hypothalamic brain development resulting in hyperphagia and obesity. This argument is formally difficult to exclude; however, no gross neuroanatomical defects were observed in brain sections from *Mc4r*$^{K314X/K314X}$ rats. Furthermore, direct evidence for a pharmacological etiology is provided by the modulation of feeding behavior and body weight regulation by acute or chronic administration of MC4R agonists and antagonists, as described above.

We believe that the *Mc4r*^{K314X} rat model will be of great value to study the cause of human monogenic obesity by adding the rat to the field of comparative genomics. Moreover, due to the increased size and cognitive performance of the rat as compared to mice, allowing for more complex surgeries and behavioral experiments, we believe that our rat model can help further understand the specific mechanisms that induce obesity during loss of MC4R function.

SUPPLEMENTARY MATERIAL

Supplementary material is linked to the online version of the paper at http://www.nature.com/oby

ACKNOWLEDGMENTS

We gratefully acknowledge Jeroen Korving for histological help.

DISCLOSURE

The authors declared no conflict of interest.

REFERENCES

1. Lu D, Willard D, Patel IR *et al*. Agouti protein is an antagonist of the melanocyte-stimulating-hormone receptor. *Nature* 1994;371:799–802.
2. Ollmann MM, Wilson BD, Yang YK *et al*. Antagonism of central melanocortin receptors *in vitro* and *in vivo* by agouti-related protein. *Science* 1997;278:135–138.
3. Schwartz MW, Woods SC, Porte D Jr, Seeley RJ, Baskin DG. Central nervous system control of food intake. *Nature* 2000;404:661–671.
4. Tao YX. The melanocortin-4 receptor: physiology, pharmacology, and pathophysiology. *Endocr Rev* 2010;31:506–543.
5. Cone RD. Anatomy and regulation of the central melanocortin system. *Nat Neurosci* 2005;8:571–578.
6. Vaisse C, Clement K, Durand E *et al*. Melanocortin-4 receptor mutations are a frequent and heterogeneous cause of morbid obesity. *J Clin Invest* 2000;106:253–262.
7. Farooqi IS, Yeo GS, Keogh JM *et al*. Dominant and recessive inheritance of morbid obesity associated with melanocortin 4 receptor deficiency. *J Clin Invest* 2000;106:271–279.
8. Calton MA, Ersoy BA, Zhang S *et al*. Association of functionally significant melanocortin-4 but not melanocortin-3 receptor mutations with severe adult obesity in a large North American case-control study. *Hum Mol Genet* 2009;18:1140–1147.
9. Lubrano-Berthelier C, Dubern B, Lacorte JM *et al*. Melanocortin 4 receptor mutations in a large cohort of severely obese adults: prevalence, functional classification, genotype-phenotype relationship, and lack of association with binge eating. *J Clin Endocrinol Metab* 2006;91:1811–1818.
10. Loos RJ, Lindgren CM, Li S *et al*.; Prostate, Lung, Colorectal, and Ovarian (PLCO) Cancer Screening Trial; KORA; Nurses' Health Study; Diabetes Genetics Initiative; SardiNIA Study; Wellcome Trust Case Control Consortium; FUSION. Common variants near MC4R are associated with fat mass, weight and risk of obesity. *Nat Genet* 2008;40:768–775.
11. Meyre D, Delplanque J, Chèvre JC *et al*. Genome-wide association study for early-onset and morbid adult obesity identifies three new risk loci in European populations. *Nat Genet* 2009;41:157–159.
12. Willer CJ, Speliotes EK, Loos RJ *et al*.; Wellcome Trust Case Control Consortium; Genetic Investigation of ANthropometric Traits Consortium. Six new loci associated with body mass index highlight a neuronal influence on body weight regulation. *Nat Genet* 2009;41:25–34.
13. Scherag A, Dina C, Hinney A *et al*. Two new loci for body-weight regulation identified in a joint analysis of genome-wide association studies for early-onset extreme obesity in French and German study groups. *PLoS Genet* 2010;6:e1000916.
14. Huszar D, Lynch CA, Fairchild-Huntress V *et al*. Targeted disruption of the melanocortin-4 receptor results in obesity in mice. *Cell* 1997;88:131–141.
15. Farooqi IS, Keogh JM, Yeo GS *et al*. Clinical spectrum of obesity and mutations in the melanocortin 4 receptor gene. *N Engl J Med* 2003;348:1085–1095.
16. Branson R, Potoczna N, Kral JG *et al*. Binge eating as a major phenotype of melanocortin 4 receptor gene mutations. *N Engl J Med* 2003;348:1096–1103.
17. van Boxtel R, Vroling B, Toonen P *et al*. Systematic generation of *in vivo* G protein-coupled receptor mutants in the rat. *Pharmacogenomics J* 2010; e-pub ahead of print 8 June 2010.
18. VanLeeuwen D, Steffey ME, Donahue C, Ho G, MacKenzie RG. Cell surface expression of the melanocortin-4 receptor is dependent on a C-terminal di-isoleucine sequence at codons 316/317. *J Biol Chem* 2003;278:15935–15940.
19. Hruby VJ, Lu D, Sharma SD *et al*. Cyclic lactam α-melanotropin analogues of Ac-Nle4-cyclo[Asp5, D-Phe7,Lys10] α-melanocyte-stimulating hormone-(4-10)-NH2 with bulky aromatic amino acids at position 7 show high antagonist potency and selectivity at specific melanocortin receptors. *J Med Chem* 1995;38:3454–3461.
20. Mul JD, Yi CX, van den Berg SA *et al*. Pmch expression during early development is critical for normal energy homeostasis. *Am J Physiol Endocrinol Metab* 2010;298:E477–E488.
21. Smits BM, Mudde JB, van de Belt J *et al*. Generation of gene knockouts and mutant models in the laboratory rat by ENU-driven target-selected mutagenesis. *Pharmacogenet Genomics* 2006;16:159–169.
22. Nickerson DA, Tobe VO, Taylor SL. PolyPhred: automating the detection and genotyping of single nucleotide substitutions using fluorescence-based resequencing. *Nucleic Acids Res* 1997;25:2745–2751.
23. Nijenhuis WA, Garner KM, van Rozen RJ, Adan RA. Poor cell surface expression of human melanocortin-4 receptor mutations associated with obesity. *J Biol Chem* 2003;278:22939–22945.
24. Brakkee JH, Wiegant VM, Gispen WH. A simple technique for rapid implantation of a permanent cannula into the rat brain ventricular system. *Lab Anim Sci* 1979;29:78–81.
25. Gispen WH, Wiegant VM, Greven HM, de Wied D. The induction of excessive grooming in the rat by intraventricular application of peptides derived from ACTH: structure-activity studies. *Life Sci* 1975;17:645–652.
26. Fan W, Boston BA, Kesterson RA, Hruby VJ, Cone RD. Role of melanocortinergic neurons in feeding and the agouti obesity syndrome. *Nature* 1997;385:165–168.
27. Kim MS, Rossi M, Abusnana S *et al*. Hypothalamic localization of the feeding effect of agouti-related peptide and alpha-melanocyte-stimulating hormone. *Diabetes* 2000;49:177–182.

28. Rossi M, Kim MS, Morgan DG *et al*. A C-terminal fragment of Agouti-related protein increases feeding and antagonizes the effect of α-melanocyte stimulating hormone *in vivo*. *Endocrinology* 1998;139:4428–4431.
29. Adan RA, Szklarczyk AW, Oosterom J *et al*. Characterization of melanocortin receptor ligands on cloned brain melanocortin receptors and on grooming behavior in the rat. *Eur J Pharmacol* 1999;378:249–258.
30. Hagan MM, Rushing PA, Benoit SC, Woods SC, Seeley RJ. Opioid receptor involvement in the effect of AgRP-(83–132) on food intake and food selection. *Am J Physiol Regul Integr Comp Physiol* 2001;280: R814–R821.
31. Koegler FH, Schaffhauser RO, Mynatt RL, York DA, Bray GA. Macronutrient diet intake of the lethal yellow agouti (Ay/a) mouse. *Physiol Behav* 1999;67:809–812.
32. Tracy AL, Clegg DJ, Johnson JD, Davidson TL, Benoit SC. The melanocortin antagonist AgRP (83–132) increases appetitive responding for a fat, but not a carbohydrate, reinforcer. *Pharmacol Biochem Behav* 2008;89:263–271.
33. Butler AA, Marks DL, Fan W *et al*. Melanocortin-4 receptor is required for acute homeostatic responses to increased dietary fat. *Nat Neurosci* 2001;4:605–611.
34. Hinney A, Schmidt A, Nottebom K *et al*. Several mutations in the melanocortin-4 receptor gene including a nonsense and a frameshift mutation associated with dominantly inherited obesity in humans. *J Clin Endocrinol Metab* 1999;84:1483–1486.
35. Ste Marie L, Miura GI, Marsh DJ, Yagaloff K, Palmiter RD. A metabolic defect promotes obesity in mice lacking melanocortin-4 receptors. *Proc Natl Acad Sci USA* 2000;97:12339–12344.
36. Hagan MM, Rushing PA, Pritchard LM *et al*. Long-term orexigenic effects of AgRP-(83–132) involve mechanisms other than melanocortin receptor blockade. *Am J Physiol Regul Integr Comp Physiol* 2000;279:R47–R52.
37. Chen AS, Marsh DJ, Trumbauer ME *et al*. Inactivation of the mouse melanocortin-3 receptor results in increased fat mass and reduced lean body mass. *Nat Genet* 2000;26:97–102.
38. Atalayer D, Robertson KL, Haskell-Luevano C, Andreasen A, Rowland NE. Food demand and meal size in mice with single or combined disruption of melanocortin type 3 and 4 receptors. *Am J Physiol Regul Integr Comp Physiol* 2010;298:R1667–R1674.
39. Irani BG, Xiang Z, Yarandi HN *et al*. Implication of the melanocortin-3 receptor in the regulation of food intake. *Eur J Pharmacol* 2011; e-pub ahead of print 1 Jan 2011.
40. Renquist BJ, Lippert RN, Sebag JA, Ellacott KL, Cone RD. Physiological roles of the melanocortin MC(3) receptor. *Eur J Pharmacol* 2011; e-pub ahead of print 3 January 2011.